IEEE Access
Multidisciplinary | Rapid Review | Open Access Journal

Received October 27, 2019, accepted November 12, 2019, date of publication November 15, 2019,
date of current version November 27, 2019.

Digital Object Identifier 10.1109/ACCESS.2019.2953756

Improved Three-Dimension Mathematical Model for Voltage Inversion of AC Overhead Transmission Lines

DONGPING XIAO[1], TAO HE[1], WENHAN ZHAO[1], XUEFEI DU[2], AND YUTONG XIE[3]

[1]State Key Laboratory of Power Transmission Equipment and System Security and New Technology, Chongqing University, Chongqing 400044, China
[2]Chongqing College of Electronic Engineering, Chongqing 401331, China
[3]Urban Power Supply Branch of State Grid Chongqing Electric Power Company, Chongqing 400015, China

Corresponding author: Dongping Xiao (xiaodongping@cqu.edu.cn)

This work was supported by the National "111" Project of China under Grant B08036.

ABSTRACT The voltages on the AC overhead transmission lines (OTLs) can be calculated inversely based on the measured electric field around the lines, which will much contribute to the non-contact condition monitoring of OTLs. To more realistically simulate the actual operating state of OTLs in the wild, a refined catenary equation of OTL with consideration of the vertical suspension and horizontal deflection is established, and the according improved three-dimensional electric field mathematical model are proposed. Furthermore, the OTLs' voltages are calculated based on an improved optimization algorithm that combines particle swarm algorithm and genetic algorithm. Some simulation and experiment cases by setting different measurement errors and wind speeds are employed to verify the improving effect of the proposed model. The analysis results shown that the three-phase maximum amplitude error is 6.48% and maximum phase error is 6.26° when the electric field measuring error is as high as 20% (beyond the normal level); on the other hand, the maximum amplitude error and phase error are 2.54% and 0.96° respectively when the wind speed is set to the strong wind of 15m/s. The results demonstrate the accuracy and robustness of the proposed model.

INDEX TERMS Overhead transmission lines (OTLs), three-dimension electric field mathematical model, accuracy of inversion, non-contact condition monitoring.

I. INTRODUCTION

The amplitudes and phase-differences of three-phase voltages are the characteristic parameters for indicating the operating state of AC overhead transmission lines (OTLs). Generally, the OTLs' voltages are measured by the potential transformers that are direct contacting with high-voltage OTLs. This traditional voltage measurement method has shown some defects in engineering application [1], [2], such as the requirement for power outage during installation and overhaul, inducing frequent core saturation or ferroresonance, causing severe insulation aging or failure, etc. Therefore, it is crucial to develop new OTLs' voltage measurement methods in the face of the development of smart grid.

In accordance with the significant correlation [3]–[6] between the voltages and electric field of OTLs, a new idea is proposed to realize the non-contact measurement of OTLs' voltages by inverse calculation based on the electric field data measured around OTLs [7]. The inverse calculation is regarded as a multi-objective optimization process embedded with OTLs' electric field calculation, in which the measured electric field data are used as the input and the OTLs' voltages are the target of optimization. This non-contact voltage measurement method has some self-evident advantages in safety and convenience [8]–[10], which would be much more useful for the on-line monitoring of OTLs' operating state.

To apply this new method in practical engineering, the accuracy and robustness of inverse calculation need to be improved. With further researches, there are mainly two aspects to promotion. On one hand, with consideration of the complex optimizing computation, the multi-objective optimization algorithm and constraint conditions can be improved and the latest relevant study can be seen in [8]. On the other hand, an improved OTLs' electric field calculation model, which takes more actual operating conditions of the OTLs and environmental factors into account, promotes

The associate editor coordinating the review of this manuscript and approving it for publication was Xiaodong Liang.

the effect of non-contact measurement. This paper focuses on the latter.

For different purposes, some researchers have established the mathematical models to calculate the electric field around OTLs. The simplest model is to regard the overhead conductor as infinite straight line and parallel to the ground, and the two-dimensional electric field can be calculated fleetly [11], [12]. Obviously, the calculation accuracy of the simplified model is hardly satisfactory. Thus, based on the catenary equation of overhead conductors, the three-dimensional electric field calculation models are established in [13]–[19]. Furthermore, the unequal suspension height and uneven span are taken into consideration in [20]–[22]. The improvements mentioned above focus on the mathematical representation of overhead conductors in the vertical direction and the consequential integral calculation method;

However, the horizontal deviation of OTLs and its impact on the spatial electric field have hardly been mentioned yet. Inevitably, operating in the wild, the OTLs are affected by the wind which produces horizontal deviation. If the real-time measured electric fields are generated by OTLs with horizontal deviation, while this factor isn't embodied in the electric field calculation model, there would be a large difference between the inversion voltages and the actual operating voltages. Subsequently, as important basis for fault diagnosis and location, the non-contact measured voltage may lead to misjudgments in on-line condition monitoring of OTLs' operating states, such as three-phase balance anomaly, single-phase grounding fault and so on. Therefore, to further improve the accuracy of inverse calculation, this paper presents a modified three-dimensional electric field calculation model with consideration of both the vertical suspension and horizontal deviation of OTLs. The effect of the improved model is discussed by theoretical error analysis.

After that, an optimization algorithm embedding with the improved electric field mathematical model is used for the voltage inversion calculation. To improve the convergence speed and calculation stability, the improved algorithm [8] absorbs the advantages of particle swarm algorithm and genetic algorithm. The voltage value can be calculated point by point in the time domain according to the mathematical models and the optimization algorithm. The characteristic parameters of sinusoidal voltages can be determined by the sinusoidal function fitting.

Several simulation cases are set to demonstrate the performance of the proposed improved model. Furthermore, an experiment system including three self-made real-time electric field measurement devices is built. According to the measuring electric field data, the voltages of OTLs with wind deviation can be effectively inversed. The simulative and experiment cases show conspicuous promotion of proposed improved model.

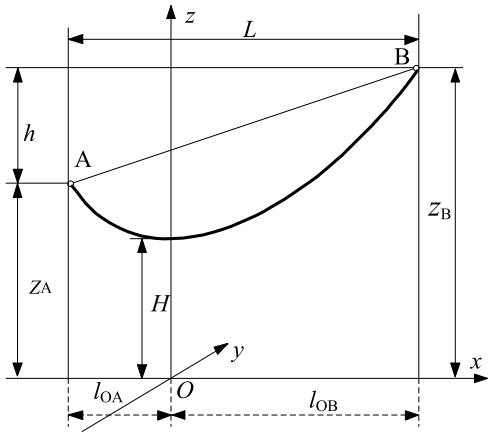

FIGURE 1. Transmission line unequal suspension diagram.

II. IMPROVEMENT OF ELECTRIC FIELD THREE-DIMENSIONAL CALCULATION MODEL CONSIDERING HORIZONTAL WIND DEFLECTION

A. OTL'S CATENARY EQUATION WITHOUT HORIZONTAL WIND DEFLECTION

The OTLs suspended between two towers are catenary. The three-dimensional OTLs diagram is set as shown in Figure 1. A and B are the two unequal suspension points with height difference of h; H is the lowest sag height and L is the span length.

The catenary equation [19]–[21] of OTL with unequal suspension is

$$z = \frac{\sigma}{\gamma}\left(\cosh\frac{\gamma x}{\sigma} - 1\right) + H \tag{1}$$

where γ and σ are the specific load and the horizontal stress of conductors, respectively.

When $x = -l_{\mathrm{OA}}$, $z = Z_{\mathrm{A}}$ and $x = l_{\mathrm{OB}}$, $z = Z_{\mathrm{B}}$. (2) can be obtained by applying these boundary conditions into (1):

$$\begin{cases} l_{OA} = \dfrac{L - \dfrac{2\sigma}{\gamma}\cdot\operatorname{arcsinh}\left[\dfrac{h\gamma}{2\sigma}\left(\sinh\dfrac{\gamma L}{2\sigma}\right)^{-1}\right]}{2} \\ l_{OB} = \dfrac{L + \dfrac{2\sigma}{\gamma}\cdot\operatorname{arcsinh}\left[\dfrac{h\gamma}{2\sigma}\left(\sinh\dfrac{\gamma L}{2\sigma}\right)^{-1}\right]}{2} \end{cases} \tag{2}$$

When the OTL is suspended with equal height, i.e. $h = 0$ and $l_{\mathrm{OA}} = l_{\mathrm{OB}} = L/2$, it means the lowest point of the sag is at the center of a span.

B. OTL'S CATENARY EQUATION WITH HORIZONTAL WIND DEFLECTION

For the OTLs operating in the wilds, the OTL's weight produces vertical specific load γ_1, and the wind pressure that is transverse to OTLs, produces the horizontal specific load γ_2. And γ_3 is a comprehensive specific load comprised with γ_1 and γ_2. These specific loads can be calculated according

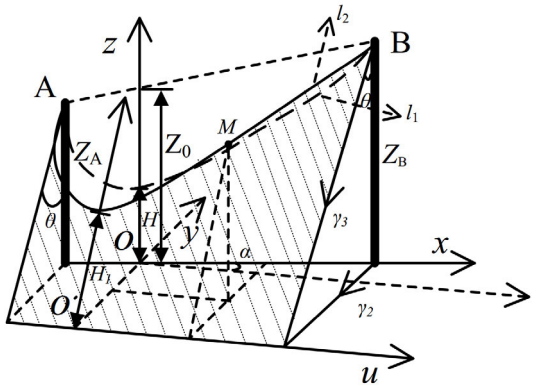

FIGURE 2. Schematic diagram of OTLs with wind deflection.

to [23], [24].

$$\gamma_2 = 0.6125 \times \frac{k_c d v_w^2}{s} \times 10^{-3} \tag{3}$$

$$\gamma_3 = \sqrt{\gamma_1^2 + \gamma_2^2} \tag{4}$$

where k_c is a constant, d and s are the dimeter and cross-sectional area of OTL respectively, and v_w represents wind speed.

In addition, the environmental temperature t will affect the horizontal stress σ of the conductor. They have the following relationship [22], [26].

$$\begin{cases} \sigma_{II}^2(\sigma_{II} + A) - B = 0 \\ A = \dfrac{e_0\gamma_I^2 L^2}{24\sigma_I^2} - \sigma_I + \kappa e_0(t_{II} - t_I) \\ B = \dfrac{e_0\gamma_{II}^2 L^2}{24} \end{cases} \tag{5}$$

where L is the length of span, κ is expansion coefficient of conductor, e_0 is elasticity coefficient, and the subscripts I and II represent two types of environmental and load conditions. Generally, I represents the known standard state.

The established xyz coordinate system and uyv coordinate system are both shown in Figure 2.

l_1 is the OTL without wind deflection and it is in the xoy plane, while l_2 shows the spatial morphology of l_1 affected by the wind and it is in the $uo'v$ plane. The wind deflection angel θ between the xoz and $uo'v$ is

$$\tan\theta = \frac{\gamma_2}{\gamma_1} \tag{6}$$

The catenary equation of l_2 in the uyv coordinate system can be calculated as follow

$$v = \frac{\sigma'}{\gamma_3}(\cosh\frac{\gamma_3 u}{\sigma'} - 1) + H_1 \tag{7}$$

where the H_1 is the lowest sag height of l_2. Considering the unequal suspension, there is an angle α between u axis and x axis

$$\frac{Z_B - Z_A}{L} \cdot \tan\theta = \tan\alpha \tag{8}$$

In this condition, the horizontal stress σ' of l_2 is

$$\sigma' = \frac{1}{\cos\alpha}\sigma \tag{9}$$

Since the electric field is measured in xyz coordinate system, l_2 should also be represented in xyz coordinate system for the convenience of analysis.

$$\begin{cases} z = \dfrac{\gamma_1}{\gamma_3} \cdot [\dfrac{\sigma'}{\gamma_3}(\cosh\dfrac{\gamma_3 x}{\sigma} - 1) + H_1] \\ y = -\dfrac{\gamma_2}{\gamma_3} \cdot [\dfrac{\sigma'}{\gamma_3}(\cosh\dfrac{\gamma_3 x}{\sigma} - 1) + H_1] + x\tan\alpha + Z_0\dfrac{\gamma_2}{\gamma_1} \end{cases} \tag{10}$$

where

$$Z_0 = \frac{Z_A \cdot l_{OB} + Z_B \cdot l_{OA}}{l_{OB} + l_{OA}} \tag{11}$$

$$H_1 = H + Z_0 \cdot (\frac{1}{\cos\theta} - 1) \tag{12}$$

In particular, when OTL is equal suspension, $Z_A = Z_B = Z_0$, and $\alpha = 0$.

C. THREE-DIMENSIONAL CALCULATION MODEL OF ELECTRIC FIELD AROUND AC OTLS

The potential in space generated by OTLs can be calculated based on the Charge Simulation Method (CSM) [27]–[30]. In numerical calculation, the catenary OTLs are discretized into small segments for linearization, and numerical integration algorithm is adopted. Then the mathematical relationship between OTLs voltages $\boldsymbol{U}$ and simulated line charges $\boldsymbol{Q}$ can be expressed in matrix form

$$\boldsymbol{U} = \boldsymbol{\lambda Q} \tag{13}$$

where $\boldsymbol{\lambda}$ is potential coefficient matrix, and its element λ_{nm} can be calculated according to mirror principle

$$\lambda_{nm} = \frac{1}{4\pi\varepsilon_0}\int_{\ell_n}\left(\frac{1}{r_{nm}} - \frac{1}{r'_{nm}}\right)d\ell_n \tag{14}$$

where ε_0 is air dielectric constant, ℓ_n is the nth segment of OTL path described in (10), r_{nm} and r'_{nm} are the distances between the nth and mth segment line charge and mth segment mirror line charge, respectively.

$$\begin{cases} r_{nm} = \sqrt{(x_n - x_m)^2 + (z_n - z_m + R_{eq})^2} & (n = m) \\ r_{nm} = \sqrt{(x_n - x_m)^2 + (y_n - y_m)^2 + (z_n - z_m)^2} & (n \neq m) \end{cases} \tag{15a}$$

$$\begin{cases} r'_{nm} = \sqrt{(x_n - x_m)^2 + (z_n + z_m - R_{eq})^2} & (n = m) \\ r'_{nm} = \sqrt{(x_n - x_m)^2 + (y_n - y_m)^2 + (z_n + z_m)^2} & (n \neq m) \end{cases} \tag{15b}$$

where the R_{eq} is the equivalent radius of a cluster of split conductors.

The electric field can be calculated

$$\begin{aligned} \boldsymbol{E} &= -\nabla v = -\left(\frac{\partial v}{\partial x}\boldsymbol{e}_x + \frac{\partial v}{\partial y}\boldsymbol{e}_y + \frac{\partial v}{\partial z}\boldsymbol{e}_z\right) \\ &= E_x\boldsymbol{e}_x + E_y\boldsymbol{e}_y + E_z\boldsymbol{e}_z \end{aligned} \tag{16}$$

The three dimensional components of electric field under power lines can be measured respectively. Some studies [31], [32] show that when the electric field measuring point is near to the ground, E_z is much larger than E_x and E_y. To ensure the accuracy of inversion calculation and reduce the complexity of optimization algorithm, the objective function of the optimization process is constructed by adopting E_z component only.

It is assumed that there are K electric field measuring points below the OTLs, and the mathematical relations between the E_z components from those measuring points and simulated line charges can be shown as

$$\boldsymbol{E}_z = \boldsymbol{B}\boldsymbol{Q} \tag{17}$$

where $\boldsymbol{B}$ is the electric field coefficient matrix, and its element b_{km} can be calculated as follow:

$$b_{km} = \frac{L}{4\pi\varepsilon_0 M}\cosh\frac{\sigma_0 x_m}{\gamma_3}\left[\frac{z-z_m}{d_{km}^3} - \frac{z+z_m}{d_{km}'^3}\right] \tag{18}$$

where d_{km} and d'_{km} are the distances between the kth measuring point and mth segment line charge and mth segment mirror line charge, respectively. M is the segmentation number of OTL in one spacing.

Eventually, the relationship between OTLs' voltages and their generated space electric field component can be obtained by synthesizing (13) and (17)

$$\boldsymbol{E}_z = \boldsymbol{B}\boldsymbol{\lambda}^{-1}\boldsymbol{U} = \boldsymbol{C}\boldsymbol{U} \tag{19}$$

III. ERROR ANALYSIS OF THE CALCULATION MODEL

The calculation based on the model without considering the wind deviation is represented with subscript 1, while the calculation based on the model considering the wind deviation is represented with subscript 2.

When the wind deviation occurs, the difference in the parameters of $\boldsymbol{\lambda}$ and $\boldsymbol{B}$ leads to the error. According to the proposed improvement shown in (10), and the parameters calculation in (14) and (18), the approximate relation of parameters of the two models is

$$\boldsymbol{\lambda}_2 \approx (\frac{\cos\theta}{\cos\alpha})^2\boldsymbol{\lambda}_1$$
$$\boldsymbol{B}_2 \approx \frac{\cos\theta}{\cos\alpha}\boldsymbol{B}_1$$

In addition, according to (8), $0 \le \alpha < \theta < 90°$, for convenience of description, there is

$$\zeta = \frac{\cos\theta}{\cos\alpha} < 1$$

The actual voltage of OTLs are assumed as $\boldsymbol{U}$ and the inverse calculated voltage $\boldsymbol{U}_1^*$ can be expressed as

$$\boldsymbol{U}_1^* = \left(\boldsymbol{B}_1\boldsymbol{\lambda}_1^{-1}\right)^{-1}\boldsymbol{E}_z = \left(\boldsymbol{\lambda}_1\boldsymbol{B}_1^{-1}\boldsymbol{C}\right)\boldsymbol{U}$$

And the error $\Delta\boldsymbol{U}_1^*$ becomes:

$$\Delta\boldsymbol{U}_1^* = \boldsymbol{U}_1^* - \boldsymbol{U} = \left(\boldsymbol{\lambda}_1\mathbf{B}_1^{-1}\boldsymbol{C} - \boldsymbol{I}\right)\boldsymbol{U}$$

Considering that there are K electric field measuring points, the corresponding error variance a_1 is

$$a_1 = \frac{\Delta\boldsymbol{U}_1^{*T}\cdot\Delta\boldsymbol{U}_1^*}{K} = \frac{\boldsymbol{U}^T\left((\boldsymbol{\lambda}_1\boldsymbol{B}_1^{-1}\boldsymbol{C})^T - \boldsymbol{I}\right)\cdot\left(\boldsymbol{\lambda}_1\boldsymbol{B}_1^{-1}\boldsymbol{C} - \boldsymbol{I}\right)\boldsymbol{U}}{K}$$

a_2 can be obtained in the same way:

$$a_2 = \frac{\boldsymbol{U}^T\left(\zeta(\boldsymbol{\lambda}_1\boldsymbol{B}_1^{-1}\boldsymbol{C})^T - \boldsymbol{I}\right)\cdot\left(\zeta\boldsymbol{\lambda}_1\boldsymbol{B}_1^{-1}\boldsymbol{C} - \boldsymbol{I}\right)\boldsymbol{U}}{K}$$

These lead to

$$a_2 < a_1$$

It shows that the improved model can increase the accuracy of calculation.

IV. OPTIMIZATION ALGORITHE FOR THE INVERSION

There are several optimization algorithms proposed for different application conditions. In this voltage inversion calculation, a single optimization algorithm can hardly meet the calculation demands of convergence speed and global optimum solution. In this paper, an improved optimization algorithm is used for inverse calculation. By absorbing the advantages of the particle swarm and genetic algorithm, the intermingled algorithm achieves a good balance between the high convergence stability and fast convergence rate. Furthermore, it resolves the issue of trapping in a local optimal solution during the rapid convergence process. The optimization algorithm is elaborated in [8], therefore, only its flow chart is shown here.

V. SIMULATION AND EXPERIMENT

A. SIMULATION ANALYSIS

1) SIMULATION CONDITION SETTINGS

According to the analysis in section II, $\boldsymbol{\lambda}$ and $\boldsymbol{B}$ are coefficient matrixes that contain the structural information of OTLs, which means the applicability for different arrangements of conductors. In addition, the voltage of multi-circuit transmission lines can be calculated with adjustment of measuring points. Here one typical case is offered. For 220kV single-circuit three-phase OTLs, the phase conductor is 2×LGJ-400/35, the radius of sub-conductor is 13.41mm, the distance of two sub-conductors in same phase is 0.35m, the span length is 200m, and the height difference between two unequal suspension points is 5m. The layout of the phase conductors at the lower tower is shown in Figure 4. The weather is sunny and the ambient temperature is 20°C.

The symmetrical three-phase voltages on OTLs are set as

$$\begin{bmatrix}\dot{U}_A\\ \dot{U}_B\\ \dot{U}_C\end{bmatrix} = \begin{bmatrix}127.02\angle -120°\\ 127.02\angle 0°\\ 127.02\angle 120°\end{bmatrix}\text{kV}$$

TABLE 1. Result of OTLS inversed voltages with no wind deflection.

Electric field measurement error	$\dot{U}_A^*$ /kV	$\dot{U}_B^*$ /kV	$\dot{U}_C^*$ /kV	maximum amplitude deviation	maximum phase error
±5%	127.1∠-119.89°	128.5∠-1.27°	126.8∠118.82°	1.13%	1.27°
±10%	126.0∠-119.32°	131.1∠2.87°	126.7∠121.04°	3.19%	2.87°
±15%	129.2∠-120.65°	122.3∠3.25°	126.3∠121.20°	3.78%	3.25°
±20%	129.9∠-116.16°	131.9∠4.08°	130.6∠120.69°	3.80%	4.08°

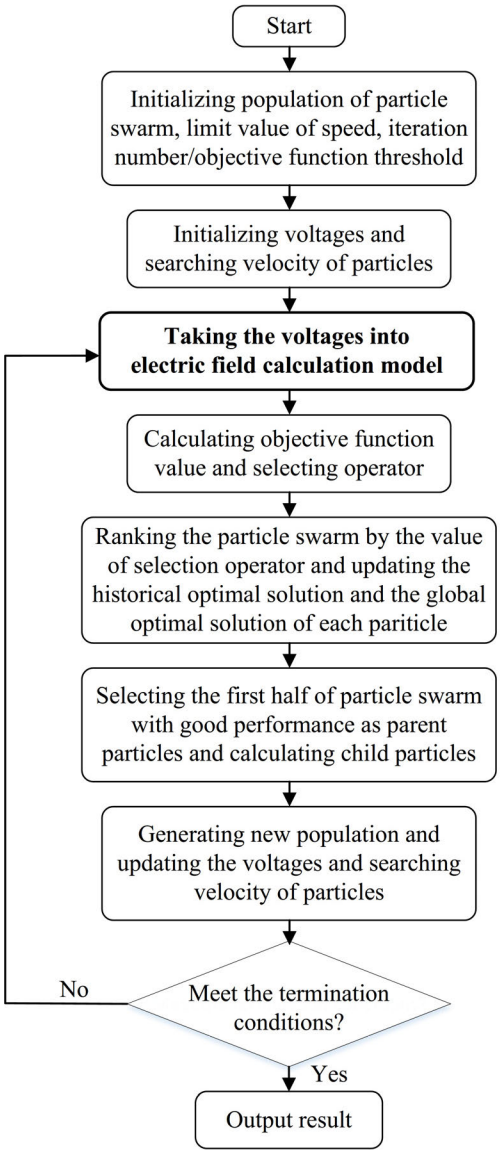

FIGURE 3. Flow chart of OTLs voltage inversion operation.

2) VOLTAGE INVERSION IN THE CONDITION WITHOUT WIND DEFLECTION

When the OTLs are operating in the normal state without wind deflection, there are $\theta = \alpha = 0$ in the proposed mathematical model, then it is the same as the conventional mathematical model.

The electric field measurement errors and random interference are inevitable in practical application. In the simulative cases, different degrees of random noise are superposed in the theoretical value of electric field to simulate the errors. Generally, the measuring error of measuring device is limited to 10% [10], [33]. In this paper, the maximum measuring error is set as 20% with consideration of random interference. The voltage inversion results and related statistical data are shown in Table I.

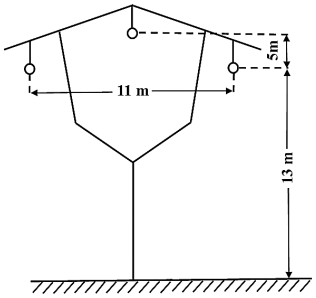

FIGURE 4. Phase conductor arrangement.

According to Table I, the three-phase maximum amplitude and phase errors increase when the electric field measurement error increases. Even if the measurement error reaches to 20%, the three-phase maximum amplitude error is limited to 3.80% and maximum phase error is 4.08°, which verified the robustness and accuracy of proposed optimization algorithm.

3) VOLTAGE INVERSION IN THE CONDITION WITH WIND DEFLECTION

When the OTLs are affected by the wind and a horizontal deviation occurs, the electric field at the spatial observation point will change accordingly. The electric field measuring devices are used to collect the real electric field data of the site. Meanwhile, if the theoretical calculation model takes no consideration of the wind deviation, there would be a large error between the inverse voltages and actual ones. Different wind speeds and their environment conditions are shown in Table III. It can be clearly seen in Figure 5. Under the condition of 10m/s wind speed and 5% electric field measurement error, the inversion results are completely invalid. While the situation is greatly improved when applying the improved model proposed in this paper.

Under the same analysis conditions, the inversion results are shown in Figure 6.

Furthermore, according to [10], [34], the different electric field measurement errors and different wind speeds are set to testify the performance of the improved model proposed

TABLE 2. Result of inversed voltages based on the improved model with different measurement errors.

Electric field measurement error	$\dot{U}_A^*$/kV	$\dot{U}_B^*$/kV	$\dot{U}_C^*$/kV	maximum amplitude deviation	maximum phase error
±5%	126.9∠-120.63°	129.3∠-0.87°	127.1∠120.11°	1.75%	0.87°
±10%	125.5∠-121.04°	131.6∠-4.49°	129.2∠122.78°	3.56%	4.49°
±15%	126.3∠-122.09°	132.4∠-5.51°	136.6∠122.85°	4.19%	5.51°
±20%	127.9∠-122.58°	135.3∠-6.26°	126.3∠124.59°	6.48%	6.26°

TABLE 3. Wind speeds and environment conditions.

Wind speeds	Description
0.0-0.2m/s	Smoke straight up
0.3-1.5 m/s	Smoke indicating wind direction
1.6-3.3 m/s	People can feel the wind
3.4-5.4 m/s	Flags spread
5.5-7.9 m/s	Dust blown up
8.0-10.7 m/s	Little trees wobble
10.8-13.8 m/s	Wires whistling
13.9-17.1 m/s	Walking difficulty
17.2-20.7 m/s	Branches broken

TABLE 4. Result of inversed voltages based on the improved model with different wind speeds.

Wind speed	$\dot{U}_A^*$/kV	$\dot{U}_B^*$/kV	$\dot{U}_C^*$/kV	maximum amplitude deviation	maximum phase error
5m/s	128.5∠-121.11°	128.6∠1.51°	127.6∠120.11°	1.20%	1.51°
10m/s	126.9∠-120.63°	129.3∠0.87°	126.7∠119.77°	1.75%	0.87°
15m/s	127.8∠-120.86°	130.3∠-0.96°	127.2∠120.00°	2.54%	0.96°

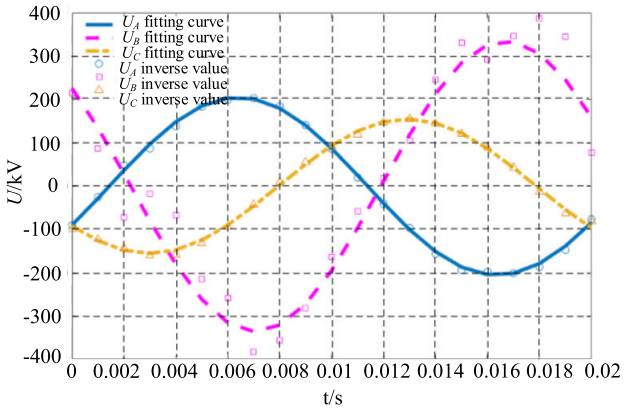

FIGURE 5. Fitting curves of inversed voltages based on the unimproved model with 5% electric field measurement error.

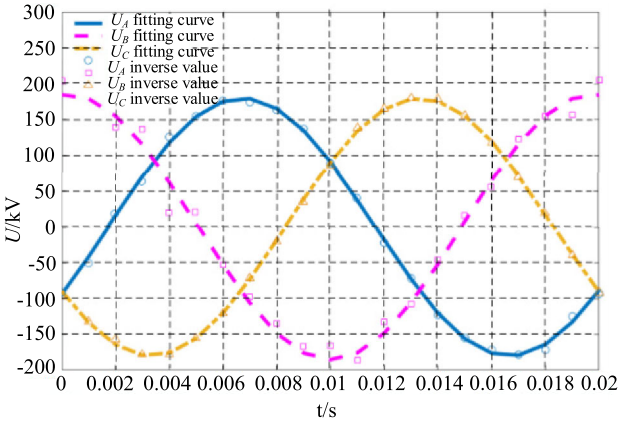

FIGURE 6. Fitting curves of inversed voltages based on the improved model with 5% electric field measurement error.

in this paper. The corresponding inversion results are shown in Tables II and IV, respectively.

Similarly, with the increase of electric field measurement error, the error of inversed voltages increases slightly as shown in Table II. Compared with Tables I and II, at the same level of measurement error, the inversion results in the presence of wind deviation are slightly larger than those in the absence of wind deviation. However, it can be seen that even under the condition with an unexpected large measurement error, the inversion results by using the proposed calculation model are still acceptable.

In this paper, 5m/s, 10m/s and 15m/s is chosen as representative wind speeds of breeze, moderate gale and strong wind shown in Table III. Bringing the wind speed into the mathematical model shown in Section II and inputting the measured electric field date under the corresponding conditions, the OTLs' voltages can be calculated. Table IV shows that under different wind conditions, accurate results can be obtained by using the proposed calculation model.

TABLE 5. Electric field data measured in the experiment (V/m).

t/ms	1	2	3	4	5	6	7	8	9	10
$E_z(1)$	-217.5	-84.8	60.08	195.17	315.54	408.65	454.96	464.47	426.32	349.97
$E_z(2)$	569.05	506.17	397.42	242.76	71.21	-107.63	-277.87	-410.4	-512.89	-558.85
$E_z(3)$	-72.23	-128.82	-171.79	-189.37	-200.82	-183.94	-150.44	-99.87	-38.24	24.92
t/ms	11	12	13	14	15	16	17	18	19	20
$E_z(1)$	237.5	105.15	-39.47	-176.17	-296.86	-383.47	-439.56	-443.26	-407.2	-328.32
$E_z(2)$	-547.32	-486.77	-373.14	-221.01	-51.54	128.56	294.84	435.41	529.89	576.57
$E_z(3)$	95.34	147.65	190.49	220.97	215.14	200.58	168.64	122.98	54.21	-10.37

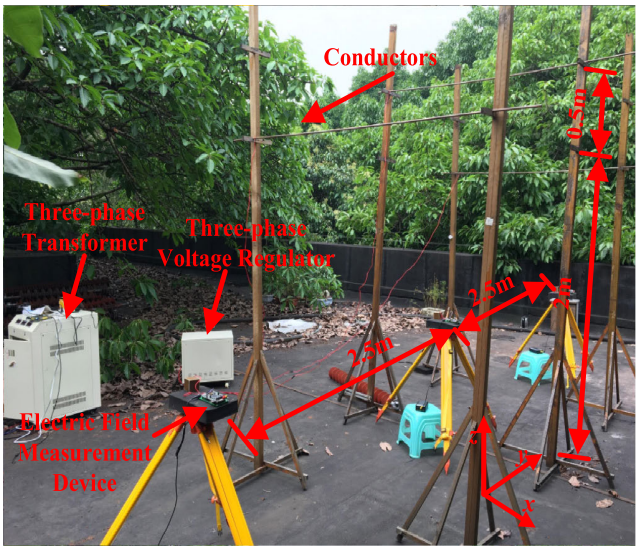

FIGURE 7. Picture of experimental site.

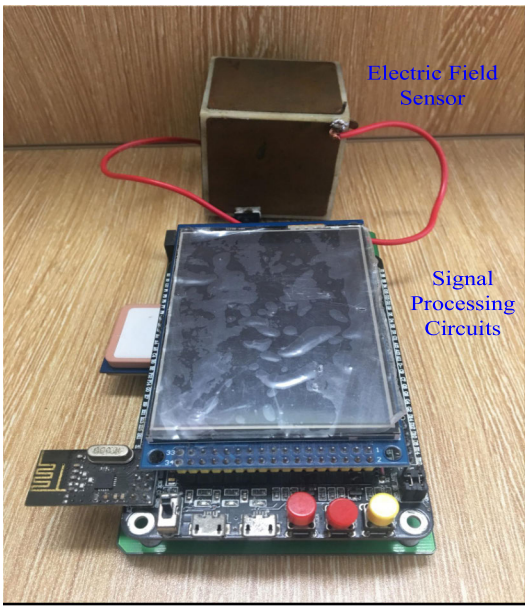

FIGURE 8. Electric field measuring device.

B. EXPERIMENTAL VERIFICATION

1) EXPERIMENTAL SETTINGS

As shown in Figure 7, the experiment system consists of a three-phase voltage regulator, a three-phase transformer, three-phase conductors, high voltage probes and oscilloscopes. In addition, three self-made real-time electric field measurement devices are designed to meet the distinctive electric field measuring requirement of multi-points, synchronization and instantaneity. The instantaneous electric field components can be measured and stored. More details about the specified electric field measuring device are elaborated in [33], and the measuring device is shown in Figure 8. The electric field measurement devices are installed at 0.9m high from the ground, with spacing distance of 2.5m from each other. The three-phase conductors are arranged at certain spatial locations to simulate the OTLs with 0.216m horizontal deflection when the wind speed is 10m/s. The three-phase voltages exerted on the conductors are actually measured by high-voltage probes and oscilloscopes, which are used to compare with the calculated voltages. Due to the influence of loads, the three-phase voltages are not completely balanced:

$$\begin{bmatrix} \dot{U}_A \\ \dot{U}_B \\ \dot{U}_C \end{bmatrix} = \begin{bmatrix} 4.01\angle -119.7^\circ \\ 3.80\angle 0.3^\circ \\ 3.61\angle 120.4^\circ \end{bmatrix} \text{kV}$$

2) EXPERIMENTAL RESULTS

The component of electric field E_z is synchronously collected by three measuring devices and the data are shown in Table V.

Taking the electric field data into voltage inversion operation algorithm based on the unimproved mathematic model, the result is

$$\begin{bmatrix} \dot{U}^*_{A1} \\ \dot{U}^*_{B1} \\ \dot{U}^*_{C1} \end{bmatrix} = \begin{bmatrix} 7.61\angle -115.6^\circ \\ 3.39\angle -21.9^\circ \\ 1.62\angle 182.9^\circ \end{bmatrix} \text{kV}$$

Obviously, the unbalance of the inversion voltages occurs. The maximum amplitude error is 89.7% and maximum phase error is 62.5°. The inversed voltages are invalid, which influences the state assessment of power lines.

While based on the improved model, the result is

$$\begin{bmatrix} \dot{U}^*_{A2} \\ \dot{U}^*_{B2} \\ \dot{U}^*_{C2} \end{bmatrix} = \begin{bmatrix} 3.95\angle -117.9^\circ \\ 3.81\angle 1.6^\circ \\ 3.47\angle 115.2^\circ \end{bmatrix} \text{kV}$$

From the above, it is clear that the maximum amplitude error decreases to 3.88% and maximum phase error is 4.8°. Compared with inversed voltage based on the unimproved model, the accuracy of inversion calculation promotes significantly.

Compared with the simulation cases, the maximum amplitude error and maximum phase error in the experiment is slightly larger than the simulation results. The result based on the improved model shows much more accuracy than that based on the unimproved model in both simulation and experiment case, which indicates the promotion effect of proposed improved electric field calculation model.

VI. CONCLUSION

In this paper, an improved electric field calculation model is proposed for the promotion of non-contact voltage measuring of OTLs. By establishing a refined catenary equation with consideration of the vertical suspension and horizontal wind deviation of OTLs, the inversion process takes more environmental factors into account and the accuracy and applicability of the non-contact measurement can be greatly improved. Verified by simulative cases with different measurement errors and wind speeds, the proposed improved electric field model shows ascent effect. In the case of OTLs with horizontal wind deflection, the inversion result obtained by the conventional calculation model is totally invalid, while based on the improved model, the three-phase maximum amplitude error is 6.48% and maximum phase error is 6.26° when the electric field measuring error is as high as 20%. Meanwhile, the three-phase maximum amplitude error is limited to 2.54% and maximum phase error is 0.96° when the strong wind speed reaches to 15m/s. In addition, the promotion effect of the proposed improved calculation model is also demonstrated by the built experiment system.

REFERENCES

[1] B. Chen, L. Du, K. Liu, X. Chen, F. Zhang, and F. Yang, "Measurement error estimation for capacitive voltage transformer by insulation parameters," *Energies*, vol. 10, no. 3, p. 357, 2017.

[2] D. Topolanek, M. Lehtonen, M. R. Adzman, and P. Toman, "Earth fault location based on evaluation of voltage sag at secondary side of medium voltage/low voltage transformers," *IET Gener., Transmiss. Distrib.*, vol. 9, no. 14, pp. 2069–2077, Nov. 2015.

[3] A. M. Farah, M. M. Afonso, J. A. Vasconcelos, and M. A. O. Schroeder, "A finite-element approach for electric field computation at the surface of overhead transmission line conductors," *IEEE Trans. Magn.*, vol. 54, no. 3, Mar. 2018, Art. no. 7400904.

[4] A. E. Tzinevrakis, D. K. Tsanakas, and E. I. Mimos, "Electric field analytical formulas for single-circuit power lines with a horizontal arrangement of conductors," *IET Gener., Transmiss. Distrib.*, vol. 3, no. 6, pp. 509–520, Jun. 2009.

[5] Y. Yang, Y. Liu, and G. Wu, "Calculation method and distribution laws of electric field on surface of overhead transmission line," *High Voltage Eng.*, vol. 41, no. 5, pp. 1644–1650, 2015.

[6] Z. Dong and T. Ashton, "Analysis of electric field influence on buildings under high-voltage transmission lines," *IET Sci. Meas. Technol.*, vol. 10, no. 4, pp. 253–258, Jul. 2016.

[7] D. Xiao, Y. Xie, H. Liu, Q. Ma, Q. Zheng, and Z. Zhan, "Position optimization of measuring points in voltage non-contact measurement of AC overhead transmission lines," *Appl. Comput. Electromagn. Soc. J.*, vol. 32, no. 10, pp. 908–914, 2017.

[8] D. Xiao, Y. Xie, Q. Ma, Q. Zheng, and Z. Zhang, "Non-contact voltage measurement of three-phase overhead transmission line based on electric field inverse calculation," *IET Gener., Transmiss. Distrib.*, vol. 12, no. 12, pp. 2952–2957, Jul. 2018.

[9] K.-L. Chen, X. Yang, and W. Xu, "Contactless voltage distortion measurement using electric field sensors," *IEEE Trans. Smart Grid*, vol. 9, no. 6, pp. 5643–5652, Nov. 2018.

[10] W. Yao, Y. Zhang, Y. Liu, M. J. Till, and Y. Liu, "Pioneer design of non-contact synchronized measurement devices using electric and magnetic field sensors," *IEEE Trans. Smart Grid*, vol. 9, no. 6, pp. 5622–5630, Nov. 2018.

[11] R. M. Sarmento, "Electric and magnetic fields in overhead power transmission lines," *IEEE Latin Amer. Trans.*, vol. 10, no. 4, pp. 1909–1915, Jun. 2012.

[12] F. Song, H. Lin, and S. Lan, "Accurate calculation of distribution of power frequency electric field for crossing UHV transmission lines," *Electr. Eng.*, vol. 17, no. 1, pp. 6–10, 2016.

[13] R. M. Radwan, M. M. Samy, M. Abdel-Salam, and A. M. Mahdy, "Electric Field Mitigation Underneath Extra High Voltage Power Lines," *IEEE Trans. Dielectr. Electr. Insul.*, vol. 20, no. 1, pp. 54–62, Feb. 2013.

[14] M. M. Samy and A. Emam, "Computation of electric fields around parallel HV and EHV overhead transmission lines in egyptian power network," in *Proc. IEEE Int. Conf. Environ. Elect. Eng. IEEE Ind. Commercial Power Syst. Europe (EEEIC)*, Milano, Italy, Jun. 2017, pp. 1–5.

[15] A. Z. El Dein, "Calculation of the electric field around the tower of the overhead transmission lines," *IEEE Trans. Power Del.*, vol. 29, no. 2, pp. 899–907, Apr. 2014.

[16] Y. Du and Y. Liao, "On-line estimation of transmission line parameters, temperature and sag using PMU measurements," *Electr. Power Syst. Res.*, vol. 93, pp. 39–45, Dec. 2012.

[17] C. P. Nicolaou, A. P. Papadakis, P. A. Razis, G. A. Kyriacou, and J. N. Sahalos, "Measurements and predictions of electric and magnetic fields from power lines," *Electr. Power Syst. Res.*, vol. 81, no. 5, pp. 1107–1116, May 2011.

[18] Z. Zou, L. Li, and X. Cui, "Calculation of the ionized field of ±800 kV high voltage DC power lines with the presence of charged atmospheric particles," *IEEE Trans. Magn.*, vol. 55, no. 10, Oct. 2019, Art. no. 7501304.

[19] Y. Wu, G. Zhao, and J. Hu, "Overhead transmission line parameter reconstruction for UAV inspection based on tunneling magnetoresistive sensors and inverse models," *IEEE Trans. Power Del.*, vol. 34, no. 3, pp. 819–827, Mar. 2019.

[20] A. Z. El Dein, M. A. A. Wahab, M. M. Hamada, and T. H. Emmary, "The effects of the span configurations and conductor sag on the electric-field distribution under overhead transmission lines," *IEEE Trans. Power Del.*, vol. 25, no. 4, pp. 2891–2902, Oct. 2010.

[21] J. C. Salari, A. Mpalantinos, and J. I. Silva, "Comparative analysis of 2- and 3-D methods for computing electric and magnetic fields generated by overhead transmission lines," *IEEE Trans. Power Del.*, vol. 24, no. 1, pp. 338–344, Jan. 2009.

[22] D.-P. Xiao, W. He, F. Yang, Z.-L. Zhang, and J. Tang, "Power frequency electric field calculation and span selection for UHV transmission lines with different meteorological conditions," *High Voltage Eng.*, vol. 35, no. 9, pp. 2081–2086, 2009.

[23] W. Wen, L. Peng, X.-W. Zhang, Y. Liu, J.-J. Ruan, Q.-J. Zhao, and X. Li, "3D power frequency electric field calculation of multi-span UHV overhead line," *High Voltage Eng.*, vol. 34, no. 9, p. 1825, 2008.

[24] W. Lou, G. Luo, and X. Yang, "Response characteristics and frequency-domain calculation method of dynamic wind-induced deflection of transmission line," *High Voltage Eng.*, vol. 43, no. 5, pp. 1493–1499, 2017.

[25] Z. Zhang, *Overhead Transmission Line Design Principle*. Beijing, China, 2010, pp. 29–30.

[26] P. Kumar and A. K. Singh, "Optimal mechanical sag estimator for leveled span overhead transmission line conductor," *Measurement*, vol. 137, pp. 691–699, Apr. 2019.

[27] J. A. Gomollon and R. Palau, "Steady state 3-D-field calculations in three-phase systems with surface charge method," *IEEE Trans. Power Del.*, vol. 20, no. 2, pp. 919–924, Apr. 2005.

[28] D. Rabah, C. Abdelghani, and H. Abdelchafik, "Efficiency of some optimisation approaches with the charge simulation method for calculating the electric field under extra high voltage power lines," *IET Gener., Transm. Distrib.*, vol. 11, no. 17, pp. 4167–4174, Nov. 2017.
[29] M. M. Samy, R. M. Radwan, and S. Akef, "Calculation of electric fields underneath and on conductor surfaces of ultra high voltage transmission lines," in *Proc. IEEE Int. Conf. Environ. Elect. Eng. IEEE Ind. Commercial Power Syst. Eur. (EEEIC)*, Milano, Italy, Jun. 2017, pp. 1–8.
[30] M. M. Samy, "Computation of electromagnetic fields around HVDC transmission line tying egypt and KSA," in *Proc. 19th Int. Middle East Power Syst. Conf. (MEPCON)*. Al Minufiyah, Egypt: Menoufia Univ., Dec. 2017, pp. 1276–1280.
[31] P. F. Mizera and J. F. Fennell, "Signatures of electric fields from high and low altitude farticles distributions," *Geophys. Res. Lett.*, vol. 4, no. 8, pp. 311–314, 1977.
[32] A. E. Tzinevrakis, D. K. Tsanakas, and E. I. Mimos, "Analytical calculation of the electric field produced by single-circuit power lines," *IEEE Trans. Power Del.*, vol. 23, no. 3, pp. 1495–1505, Jul. 2008.
[33] H. T. Liu, "Study on power-frequency electric field measurement method for inverse calculation voltages of overhead transmission lines," (in Chinese), M.S. thesis, College Elect. Eng., Chongqing Univ., Chongqing, China, 2016, pp. 22–36.
[34] X. Ma, Y. Jin, and Q. Dong, "A generalized dynamic fuzzy neural network based on singular spectrum analysis optimized by brain storm optimization for short-term wind speed forecasting," *Appl. Soft. Comput.*, vol. 54, pp. 296–312, May 2017.

DONGPING XIAO was born in Xuanwei, Yunan, in 1977. She received the B.Sc. degree in industrial automation and the M.Sc. and Ph.D. degrees in electrical engineering from Chongqing University, Chongqing, China, in 1999, 2004, and 2009, respectively. From 2012 to 2013, she was a Visiting Scholar with Washington State University, USA. She is currently an Associate Professor with the College of Electrical Engineering, Chongqing University. Her research interests include the calculation and simulation of electromagnetic field, electromagnetic measurement, and running state monitoring of power transmission equipment.

TAO HE was born in Yunyang, Chongqing, in 1994. He received the B.Sc. degree in electrical engineering from the University of Electronic Science and Technology of China, Chengdu, China, in 2017. He is currently pursuing the master's degree with Chongqing University, China, with a focus on the calculation and simulation of electromagnetic field and running state monitoring of power transmission equipment.

WENHAN ZHAO was born in Jilin, China, in 1994. He received the B.Sc. degree in electrical engineering and automation from Chongqing University, in 2017. He is currently pursuing the master's degree with Chongqing University, focusing on electric field measurement and device development.

XUEFEI DU was born in Chongqing, China, in 1977. He received the B.Sc. degree in industrial automation and the M.Sc. degree in control theory and control engineering from Chongqing University, Chongqing, China, in 1999 and 2004, respectively. From 2004 to 2011, he worked in CISDI Engineering Co., Ltd. From 2011 to 2018, he worked in CISDI Electric Technology Co., Ltd. From 2019, he is a Professor with the Chongqing College of Electronic Engineering. His main research interests include intelligent instruments, electric automatization, and industrial internet.

YUTONG XIE received the B.Sc. and master's degrees in electrical engineering from Chongqing University, China, in 2015 and 2018, respectively. She is currently working as a Relay Protection Assistant Engineer with the Urban Power Supply Branch of State Grid Chongqing Electric Power Company, which takes the investment, construction and operation of power grid as the core business. Her research interests include electromagnetic environment of high voltage power system, electromagnetic inverse problem, and relay protection of electric power system.